Power output estimation of a two-body hinged raft wave energy converter using HF radar measured representative sea states at Wave Hub in the UK

Wang, Daming; Jin, Siya; Hann, Martyn; Conley, Daniel; Collins, Keri; Greaves, Deborah

Published in:
Renewable Energy

DOI:
10.1016/j.renene.2022.11.048

Publication date:
2023

Power output estimation of a two-body hinged raft wave energy converter using HF radar measured representative sea states at Wave Hub in the UK

Daming Wang[1], Siya Jin[*2], Martyn Hann[1], Daniel Conley[1], Keri Collins[1], and Deborah Greaves[1]

[1]*School of Engineering, Computing and Mathematics, Faculty of Science and Engineering, University of Plymouth, PL4 8AA, UK*

[2]*Ocean Institute, Northwestern Polytechnical University, Taicang, Jiangsu, 215400, China*

Abstract:

For the physical model testing of wave energy converters (WECs) in the wave basin, it is necessary to test the models in a small number of sea states. Previously, the $H - T$ binning method was widely used to determine the sea states that are representative of an ocean area. However, it omitted much useful information such as the wave directionality. In this paper, a novel method, the *K*-means clustering technique is used in combination with High Frequency (HF) radar measured data from Wave Hub, UK. The results show that *K*-means clustering method better preserves the characteristics of the ocean area than the binning method. Furthermore, the impact of different regrouping methods on assessing the annual energy output of the model is investigated, by applying the *K*-means clustering method to a 1:25 two-body hinged raft WEC. It is found that although non-linear performance can be clearly observed in the model both physically and numerically. Due to the fact that most sea states from Wave Hub are out of the non-linearity range of the model, the non-linear effect on the overall performance of the WEC model in this ocean area is limited. It allows the annual energy output to be accurately predicted by using only a small number of representative sea states (defined as K) $\leqslant 15$, based on *K*-means clustering method.

Key words: *K*-means clustering; binning method; HF radar; hinged raft WEC; physical modelling; WEC-Sim numerical modelling

[*] Corresponding author. Email Address: siya_jin@126.com (Siya Jin)

1. Introduction

Due to global warming and the need to combat climate change, research into renewable energy becomes more and more important. Among various types of renewable energy, marine renewable energy (MRE) is considered an energy source with high potential. MRE can be considered to consist of five types, which are wave energy, ocean current energy, tidal energy, offshore wind energy, and osmotic energy. Among these, wave energy has a high power density; the global potential being about 26,000 TW.h/year [1], which could satisfy the global annual electricity generation in 2020 of 26,889 TW.h [2] if the global exploitable wave resource can be fully harnessed.

The devices designed to capture and convert wave energy into useful power are wave energy converters (WECs). Hundreds of WECs have been designed so far, including mainly the types of the oscillating water column (OWC), the point absorber (PA), the overtopping device, and the attenuator [3]. For an attenuator WEC, it is aligned perpendicular to the wave direction and its length is comparable to the incident wavelength. Representative examples are Pelamis [4], M4 [5], SeaPower [6], Blue Star & Blue Horizon [7], etc. A two-body hinged raft WEC belonging to the attenuator type is studied in this work.

To describe the development stages to commercialize a WEC design, the technology readiness level (TRL) [8] is used. It divides the development of a WEC from concept design to commercialization into 9 TRLs and 5 stages [9], and stage 1 (TRL from 1 to 3) and stage 2 (TRL from 3 to 5) rely heavily on physical model testing with scale parameters ranging from 1:100 to 1:10 [10]. Physical model testing is an important tool for the development of WECs. However, tank time is expensive so the number of sea states tested in a campaign must be limited. It is necessary to select several representative sea states for physical model testing based on limited resources. Instruments such as wave-rider buoy, acoustic doppler current profiler (ADCP), X-band radar, and HF radar are used to measure sea states at potential deployment sites in the form of the hourly directional wave spectrum. Due to a large amount of measured data annually, selecting a certain number of sea states for model testing is important to accurately represent the wave climate.

Traditionally, the H_s-T_e (or H_s-T_p) bivariate binning method is used to identify the number of occurrences of the characterised significant wave height H_s and wave energy period T_e (or peak wave period T_p) combinations (see Fig. 1). Sea states described by these determined H_s-T_p are then input into a parametric wave spectrum such as JONSWAP or PM with the targeted wave directionality simplified by a directional spreading function (DSF) to represent the site-specific sea states [11]. However, such a method is a simplification of the actual site conditions. The real spectral shape and directional spreading may differ from these parametric wave spectra. Apart from that,

the H_s-T_p bins selected for tank testing can be non-representative because not every sea state is included in the selected bins (see Fig. 1), and thus, the traditional binning method cannot be used to represent the whole wave climate [12].

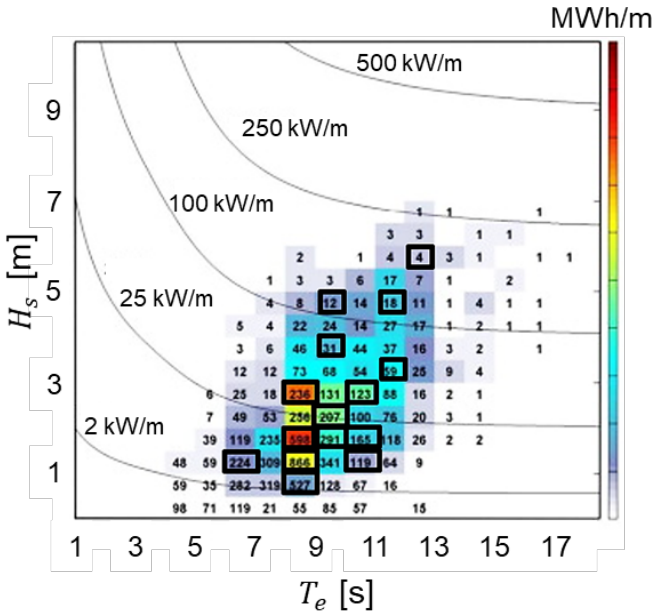

Fig.1. Representation of the traditional H_s-T_e bivariate binning diagram for the wave resource at a considered site. The bins created are of size 0.5 m × 1 s. In total, 118 non-empty bins are created, in which only 15 bins circled by solid black lines are selected for later use in tank testing. The values shown in the bins are the number of occurrences in a year for the corresponding H_s-T_e.

To obtain the sea states that can represent sufficiently the annual dataset, Hamilton applied the *K*-means clustering method (a detailed explanation of the *K*-means clustering technique is shown in Section 2) on 2456 non-directional wave spectra measured at Port Hedland, Australia in 1992 to obtain a group of representative sea states [13]. In contrast to the traditional H_s-T_p binning method, the representative sea states consider the physically measured spectral shape. The work demonstrated the viability of using the *K*-means clustering technique on sea states regrouping. This method was later extended into 8 methods which include 2 binning methods and 6 *K*-means clustering methods using different wave parameters and compared by Draycott to identify 20 and 40 representative sea states from 64673 buoy-measured half-hourly directional wave spectra obtained for the European Marine Energy Centre (EMEC) site [14]. It was found that methods based on non-directional and directional wave spectra *K*-means clustering present a smaller relative error between the cluster mean and each member in the same group created, compared to the commonly used $H - T$ binning method and the *K*-means methods only using several wave parameters. Wang [15] continued Draycott's research and compared 10 regrouping methods (with

Draycott's 8 methods, and 2 new methods based on *K*-means clustering) by using 3161 HF radar measured hourly sea states in Cornwall, UK, and 8402 floating buoy measured hourly sea states in Long Island, US to obtain representative sea states. Wang showed that the regrouping quality of the same regrouping method is regardless of the location (Cornwall or Long Island) or the measuring instrument (HF radar or floating buoy) the sea states were measured. Methods based on non-directional and directional wave spectra *K*-means clustering are better than other methods, which is the same conclusion drawn from the EMEC sea states analysis by Draycott [14].

Furthermore, to suggest the most appropriate regrouping method for the model testing design of a WEC, Wang [16] tested the representative sea states obtained from 10 regrouping methods on a linear Point Absorber (PA) RM3 numerical model in WEC-Sim [17] and estimated the power output and annual energy output. It was found that for the fully linear RM3 model, the regrouping method using *K*-means clustering based on the non-directional wave spectrum provides the representative sea states corresponding to the power output scenarios with the highest representativeness (with the lowest average difference between the cluster mean and each group member compared to other regrouping methods). The annual energy output was shown to be accurately predicted by using only 20 representative sea states. However, this conclusion prompts the question of whether the practical non-linearity of a WEC has an influence on wave regrouping and the power output performance of the device.

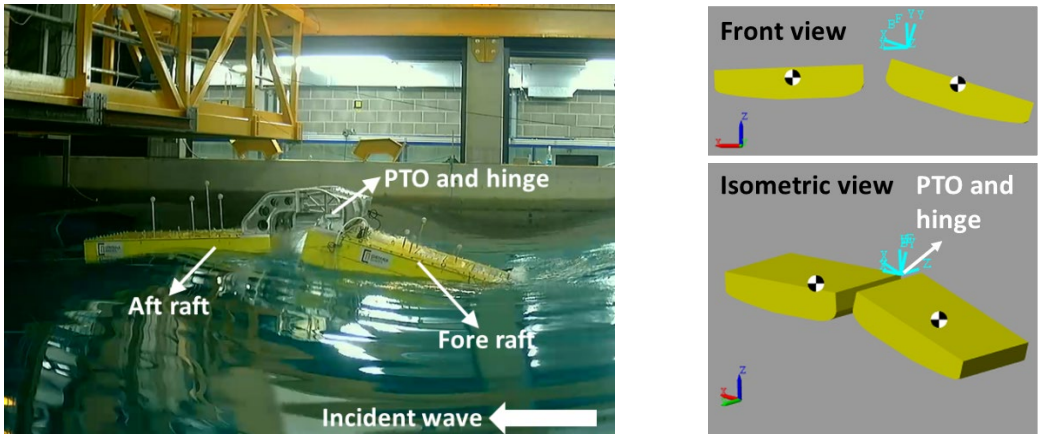

(a) (b)

Fig. 2. Physical and numerical testing of a 1:25 scale two-body hinged raft WEC. (a) The physical testing was conducted in the COAST laboratory at the University of Plymouth. The device comprises a fore raft, an aft raft, and a power take-off (PTO) system aligned with the hinge connection. (b) The numerical testing was developed in the open-source tool WEC-Sim.

To address this question, in this paper representative sea states obtained from 10 different regrouping methods (using *K*-clustering/binning method) are tested both physically and numerically with consideration of the WEC

non-linearity of a 1:25 hinged raft WEC. As shown in Fig. 2, the physical testing is conducted at the Coastal, Ocean, and Sediment Transport (COAST) laboratory at the University of Plymouth (UoP); the numerical testing is developed in WEC-Sim. To the best knowledge of the authors, this is the first time that regrouping methods are investigated physically and numerically on a WEC. The authors hope that the data provided in this work can be useful for guiding the model testing design and improving the performance estimation of a WEC. The 1: 25 hinged raft WEC was designed and manufactured as part of the Round-Robin testing under the EU H2020 MaRINET2 project, which focuses on evaluating the impact of the facility itself on the experimental results, not the design optimisation of a WEC. Detailed information on the Round-Robin testing for this hinged raft has been addressed in [18]. The remainder of the paper is structured in the following way: regrouping methods are described in Section 2; the experimental and WEC-Sim numerical testing on the hinged raft WEC are described in Section 3; results and discussion of testing different regrouping methods on this hinged raft WEC are given in Section 4; conclusions are drawn in Section 5.

2. Description of wave regrouping methods

3161 hourly sea states at Wave Hub measured by HF radar system between 04/2012 and 12/2012 are used as the total dataset in this paper. The HF radar data were obtained by a two-phased-array Wellen Radars (WERA) system located on the southwest coast of the UK, overlooking the marine renewable testing field, Wave Hub. Each measured hourly directional wave spectrum (in the units of $m^2/(Hz \cdot rad)$) is characterised by 30 angular directions ranging from 0 rad to $29\pi/15$ rad and 92 frequencies ranging from 0.03 Hz to 0.28 Hz. The HF radar system was installed and maintained by the UoP in 2021. The accuracy of the data was high with the significant wave height obtained having nearly zero bias and the relative error of the energy period within 10% [19]. Only 3161 hourly sea states between 04/2012 and 12/2012 were used, because the measured wave data with low signal-to-noise ratio were considered to be of low quality and were removed from the data set. From previous research [15], a larger data set were used (Long Island sea states with 8402 hourly sea states annually). It was found that the regrouping quality using the same regrouping methods with different data sets is almost identical. As a result, the HF radar data set with 3161 hourly sea states is used in this research. The data used is not publicly available but can be acquired with a request.

2.1. *K*-means clustering technique

K-means clustering is a method that divides a total of *N* members into *K* groups, ensuring that similar members are put in the same group by minimising the sum of squared error (SSE) of all members. SSE is expressed as [20]:

$$\mathrm{SSE} = \sum_{k=1}^{K} \sum_{x_i \in C_k} ||x_i - \mu_k||^2 = \sum_{k=1}^{K} \sum_{x_i \in C_k} d(x_i, \mu_k)^2, \quad (1)$$

where x_i is the data member, C_k is the set of members in cluster k, μ_k is the vector mean of cluster k. d is the Euclidean distance between two p-dimensional instances, where $x_i = (x_{i1}, x_{i2}, \ldots, x_{ip})$ and $x_j = (x_{j1}, x_{j2}, \ldots, x_{jp})$.

$$d(x_i, x_j) = (|x_{i1} - x_{j1}|^2 + |x_{i2} - x_{j2}|^2 + \ldots + |x_{ip} - x_{jp}|^2)^{1/2}. \quad (2)$$

μ_k is defined as:

$$\mu_k = \frac{1}{M(k)} \sum_{x_i \in C_k} x_i, \quad (3)$$

in which $M(k)$ is the number of members in C_k.

From the definition of SSE, a preferred *K*-means clustering method should be the one providing the minimum average difference SSE between group members and their cluster mean. The flow chart described in Fig. 3 is used to find the optimum *K* clusters by minimising SSE. When SSE does not decrease by relocating the cluster centres, it indicates the current partition is optimal and the iteration can stop [21], [22]. It should be noted that the iteration can also stop when SSE is below a certain defined limit. The clustering results can be affected by the selection of the *K* targets used in the first iteration. As a result, the calculation is usually repeated multiple times (replicates) and the result with the minimum SSE is considered the optimized result [23].

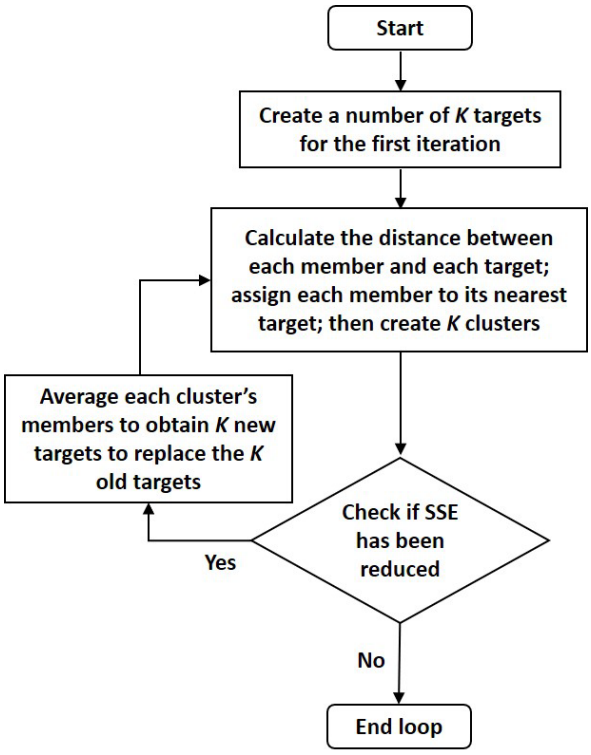

Fig.3. Workflow of the *K*-means clustering technique.

2.2. Regrouping methods

As described in Table 1, 10 regrouping methods are proposed in this work to obtain representative sea states for model testing from 3161 HF radar measured hourly sea states. The equation of each wave parameter used can be found in [14]. It can be seen that 8 out of 10 regrouping methods are based on the *K*-means clustering technique, and the other 2 are binning methods A and B. As suggested from the previous work [15]: (1) regardless of which regrouping method is used, the regrouping quality increases with *K* (number of groups) for the same total dataset; (2) when $K > 20$, increasing *K* cannot improve the regrouping quality obviously; and (3) it is not possible to increase *K* without limit, due to the time constraints of the model testing. Therefore, to compare the impact of different regrouping methods on the regrouping quality of the wave, $K = 20$ is used for methods A–J, as discussed in Sections 2.2 and 2.3.

Table 1. 10 regrouping methods. H_s is the significant wave height; T_e is the wave energy period; $\theta_m$is the mean wave direction; *S(f)* is the non-directional wave spectrum; *S(f, θ)* is the directional wave spectrum; *v* is the wave spectral bandwidth; P_w is the wave power; S_p is the wave steepness, σ_θ is the directional spreading parameter.

Serial number	Method	Parameter
A	Binning	H_s, T_e
B		H_s, T_e, θ_m
C	*K*-means clustering	*S(f)*
D		*S(f, θ)*
E		H_s, T_e
F		H_s, T_e, θ_m, v, P_w, S_p, σ_θ
G		E + C
H		F + D
I		C + modified E
J		D + modified E

As shown in the traditional binning method in Fig. 1, only 15 bins are selected for model testing, while 118 non-empty bins are created. Generally, those bins are selected subjectively. Users tend to select bins with H_s and T_e

that they are interested in according to different WECs. However, due to the loss of a large number of non-empty bins, it is difficult to determine whether the selected bins are fully representative.

To solve the problem, in this work, the bin size is determined based on the full range of H_s and T_e, instead of using the traditionally fixed bin size (e.g., 0.5 m × 1 s, as shown in Fig. 1). As described in Fig. 4, for method A in this paper, 6 and 4 bins are finally determined over the full range of H_s and T_e respectively to reach K = 20 as closely as possible. However, it can be seen that the desired number of non-empty bins is very hard to satisfy. As a result, only 19 non-empty bins are created and used in this work for method A, not 20.

Method B is like method A but with a third dimension θ_m added. Therefore, the bins created are cubic. After multiple attempts, 4, 3, and 3 bins are used over the full range of H_s, T_e and θ_m respectively to reach K = 20 as close as possible. As a result, K = 21 is achieved for method B.

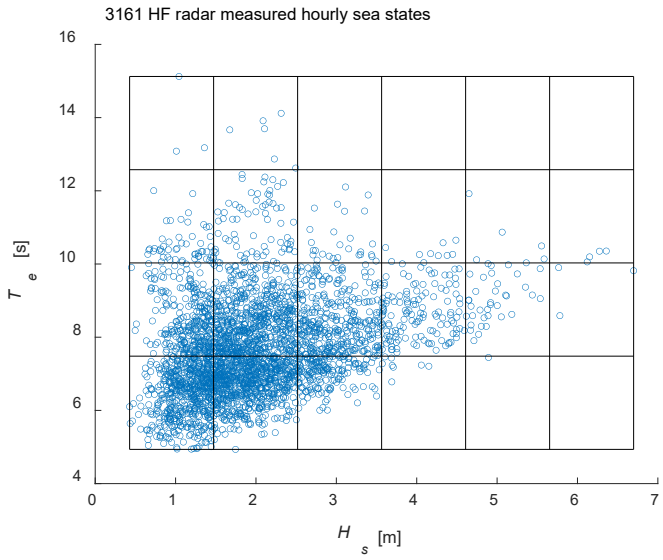

Fig.4. Diagram of method A with 24 bins created for 3161 HF radar measured hourly sea states with only 19 non-empty.

Method C is the *K*-means clustering method in terms of the non-directional wave spectrum. The difference between the two members $S_i(f)$ and $S_j(f)$, $f = (f_1, f_2, \dots, f_p)$ is given below:

$$d\big(S_i(f), S_j(f)\big) = (|S_i(f_1) - S_j(f_1)|^2 + |S_i(f_2) - S_j(f_2)|^2 + \dots + |S_i(f_p) - S_j(f_p)|^2)^{1/2}. \quad (4)$$

Method D is the directional wave spectrum *K*-means clustering method. The difference between two members $S_i(f,\theta)$, $S_j(f,\theta)$, $f = (f_1, f_2, \dots, f_p)$, $\theta = (\theta_1, \theta_2, \dots, \theta_q)$ can be calculated by:

$$d\left(S_i(f,\theta), S_j(f,\theta)\right) = \frac{1}{pq}[\sum_{m=1}^{p}\sum_{n=1}^{q}(|S_i(f_m,\theta_n) - S_j(f_m,\theta_n)|^2)]^{1/2}. \quad (5)$$

Method E is the *K*-means clustering method with normalized significant wave height H_s and energy period T_e (both of the parameters are normalized by their total mean value respectively to eliminate the influence from different units). The relative difference between two members can be obtained from Eq. (2) with H_s as x_1 and T_e as x_2.

Method F is similar to method E but considers another 5 wave parameters, all of which are normalized by the mean value of the total data set respectively. The relative difference between two members can be obtained from Eq. 2 with H_s as x_1, T_e as x_2, θ_m as x_3… and σ_θ as x_7.

Method G and H are both two-step methods in which the first step is to create *K*/2 sub-groups by method E or F and the second step is to use C and D to split each sub-cluster into two groups to obtain *K* groups in total. Method I and J are also two-step methods as well but using method C or D as the first step then using a modified method E which balances the importance of normalised H_s and T_e in the clustering process. Full details are given in [15].

After obtaining the relative difference between two members, the *K*-means clustering technique can be applied to methods C to J. To show the regrouping results clearly, methods A to J and their obtained representative sea states (i.e., the mean of the directional wave spectra of each group) for the 3161 HF radar dataset when K = 20 are plotted in H_s-T_e space in Fig. 5.

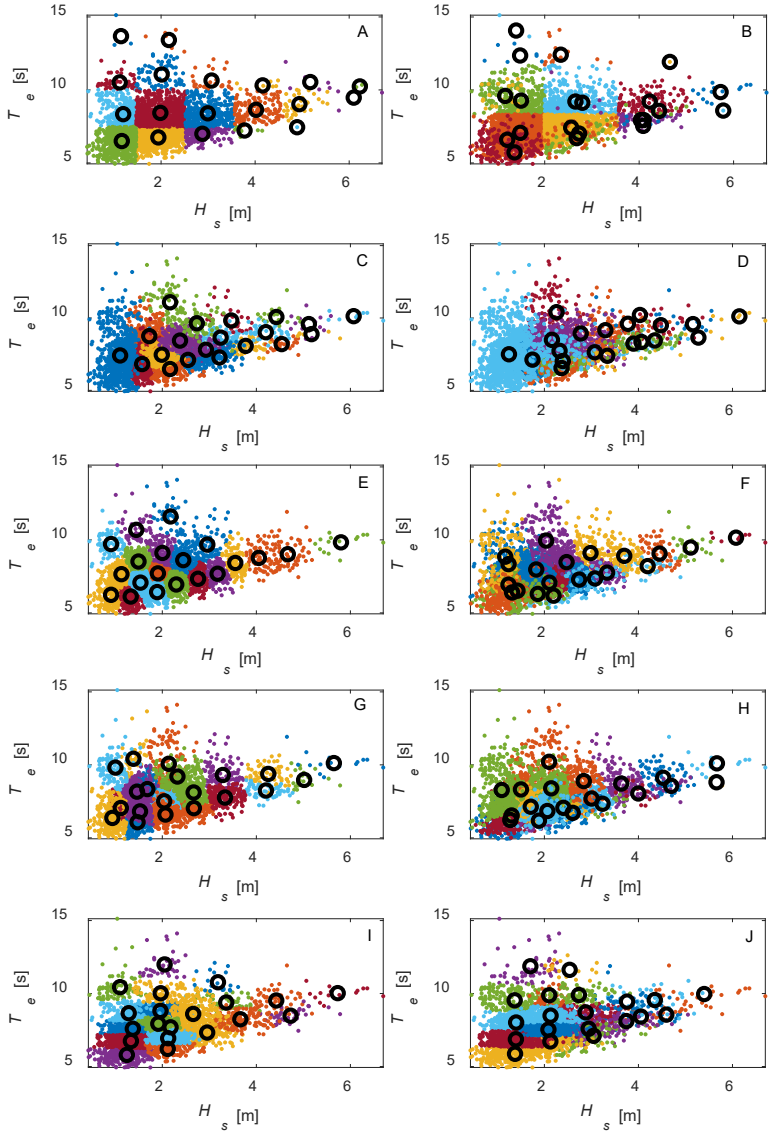

184

185 Fig.5. Wave groups created using 10 regrouping methods A to J based on the 3161 HF radar measured data for
186 Wave Hub, under K = 20. Wave scatter data assigned in the same group are marked in the same colour. The
187 corresponding representative sea states obtained are marked by black circles. For K-means methods C to J, the
188 number of maximum iterations is 200. The number of replicates is 100.

189 **2.3. Metric used to quantify the regrouping quality of different method**

190 After groups are obtained (as shown in Fig. 5), it is necessary to compare the quality of different regrouping
191 methods, and a metric proposed in [24] is used here and expressed as:

$$Met(\delta) = \sum_{k=1}^{K} \frac{1}{K} \sum_{m=1}^{M(k)} \frac{1}{M(k)} \sum_{d=1}^{D(\delta)} \frac{|\delta_{k,m,d} - \mu_{k,d}(\delta)|}{\mu_{k,d}(\delta)}, \tag{6}$$

192 in which K is the number of groups created; k = 1, 2, …, K represents each of the groups; $M(k)$ represents the
193 number of members inside group k; m = 1, 2, …, $M(k)$ represents each of the members in group k; δ represents
194 the wave parameter used for representativeness assessment, $\delta = H_s, T_e, \dots, S(f), S(f,\theta)$; d represents the number
195 of discrete values δ has, $d = 1, \dots, D(\delta)$. The value $D(\delta)$ depends on the variable δ to be analysed. For each of
196 the one-dimensional variables (H_s, T_e, v, P_W, θ_m), $D(\delta)$ = 1. For non-directional wave spectra $S(f)$ with $f =$
197 $(f_1, f_2, \dots, f_p)$,$D(\delta) = p$. For directional wave spectra $S(f,\theta)$ with $f = (f_1, f_2, \dots, f_p)$ and $\theta = (\theta_1, \theta_2, \dots, \theta_q)$,
198 $D(\delta) = p \times q$. From Eq. (6), the lower metric is, the higher the representativeness of the regrouping quality.

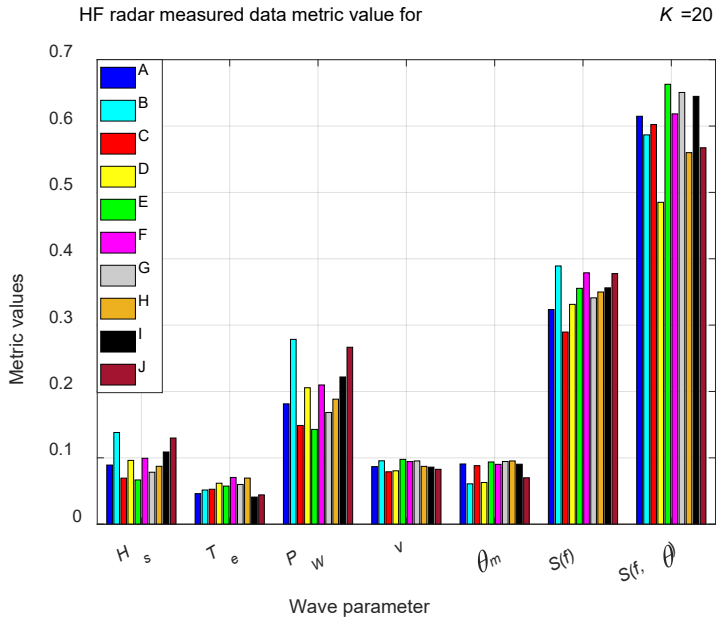

199

200 Fig.6. Metric values (from Eq. (6)) with reference to 7 wave parameters according to10 regrouping methods A to
201 J.

202 The metric values of 7 wave parameters including H_s, T_e, P_W, v, θ_m, P_w, $S(f)$, and $S(f,\theta)$ analysed through
203 methods A to J are plotted in Fig. 6 to quantify the regrouping quality of different methods. Taking the value of
204 0.2 as an example, as can be seen from Fig.6, the metric values of P_W are close to 0.2 for all 10 regrouping methods.
205 It means the average difference of P_W between the group mean value and each of the group members in the same
206 group is 20%. As observed, the metric values for one-dimensional wave parameters (H_s, T_e, P_W, v, θ_m) are lower
207 than those of p-dimensional non-directional spectra $S(f)$; the metric values for non-directional spectra are lower
208 than those of the $p \times q$ directional spectra $S(f,\theta)$. This is because of the reduction in detail by which individual
209 sea states are defined as they are integrated from $S(f,\theta)$ to $S(f)$, to one-dimensional parameters [15].

In order to clarify further the results described in Fig. 6, the results of different regrouping methods are given a rank based on their performance. The metric results are based on the comparison of the orders of magnitude of each variable in Fig. 6. The highest representativeness of 10 regrouping methods (with the lowest value among ten methods) is ranked as '1' and the lowest representativeness (the highest value) is ranked as '10', the results are shown in Table 2 below:

Table 2: The ranks of different methods of HF radar data with the lowest rank marked in blue and the highest rank marked in red.

method	H_s	T_e	P_w	v	θ_m	$S(f)$	$S(f,\theta)$	Total
A	5	3	4	5	7	2	6	32
B	10	4	10	9	1	10	4	48
C	2	5	2	1	4	1	5	20
D	6	8	6	2	2	3	1	28
E	1	6	1	10	8	6	10	42
F	7	10	7	7	5	9	7	52
G	3	7	3	8	9	4	9	43
H	4	9	5	6	10	5	2	41
I	8	1	8	4	6	7	8	42
J	9	2	9	3	3	8	3	37

By comparing ten different regrouping methods, it can be seen that among all of the seven wave parameters assessed, method C (clustering with non-directional wave spectra) provides the overall highest regrouping quality (representativeness) with the lowest total ranks (20) of the metric value, which means method C provides the overall highest representativeness (with the lowest total ranks) among ten methods, which is the same conclusion with previous research [25]. It is because method C considers the influence of the wave spectrum as a whole, whereas other methods only consider several wave parameters. It is no surprise method C provides a much better overall performance than others.

From Fig. 6 and Table 2, it can be seen that there is a relationship between the quality of a wave parameter and the degree of participation of the same wave parameters in the regrouping process. Taking mean wave direction θ_m for example, method B used θ_m directly for binning process and the representativeness of θ_m for method B is highest compared with other regrouping methods (rank 1). It is a similar result for method D. Although method D uses directional wave spectra for the clustering process without using θ_m directly. However, the directional information is included in the directional wave spectra, which means method D has wave directional information

θ_m participating in the clustering process indirectly and for this reason, method D shows a high quality for wave parameter θ_m (rank 2). Clustering method C uses the non-directional wave spectrum for regrouping, which produces representative sea states with the highest representativeness (rank 1) of the individual non-directional wave spectrum, i.e., the lowest metric value for $S(f)$. Similarly, clustering method D using the individual directional wave spectrum produces representative sea states that best represent the individual directional wave spectrum $S(f,\theta)$ with rank 1 as well.

As can be seen, the binning methods (A and B) perform less well for the majority of parameters with total ranks of 32 and 48 respectively. Method E shows high representativeness for H_s and P_w (both rank 1) but low for $S(f)$ (rank 6) and $S(f,\theta)$ (rank 10). Method F shows low representativeness for almost every wave parameter with the highest total rank values (total ranks 52) and is the first to be eliminated from use. Two-step methods G and H, show medium performance for most of the wave parameters with total ranks of 43 and 41 respectively and are also excluded from use. Method I and J are created in order to have a balance between the *K*-means clustering methods and the binning methods, which results in I and J having low performance regarding representativeness with total ranks of 41 and 37, and also need to be excluded from using.

Comparison between method C (using *K*-means clustering) and method A (using binning) for $S(f)$ are clearly described in Fig. 7. As can be seen, (1) both methods create 20 (or close to 20 for binning method A) groups and thus give 20 representative wave spectra; (2) each group contains a different series of members; (3) the generated representative waves can closely keep the real spectrum shape recorded by the HF radar system, which is shown to be different from the commonly used parametric JONSWAP or PM spectrum; (4) method C clusters the sea states with similar wave spectra $S(f)$ in the same group automatically, which is not the case for the binning method in that members are grouped based on the defined bin size.

As a result, method C is the method used for regrouping the HF radar measured sea states and tested physically on the 1:25 hinged-raft model, considering the time limit of the physical model testing. It should be noted that the 10 methods A to J are fully evaluated through the developed and validated numerical model testing, as discussed in Sections 4.2 and 4.3.

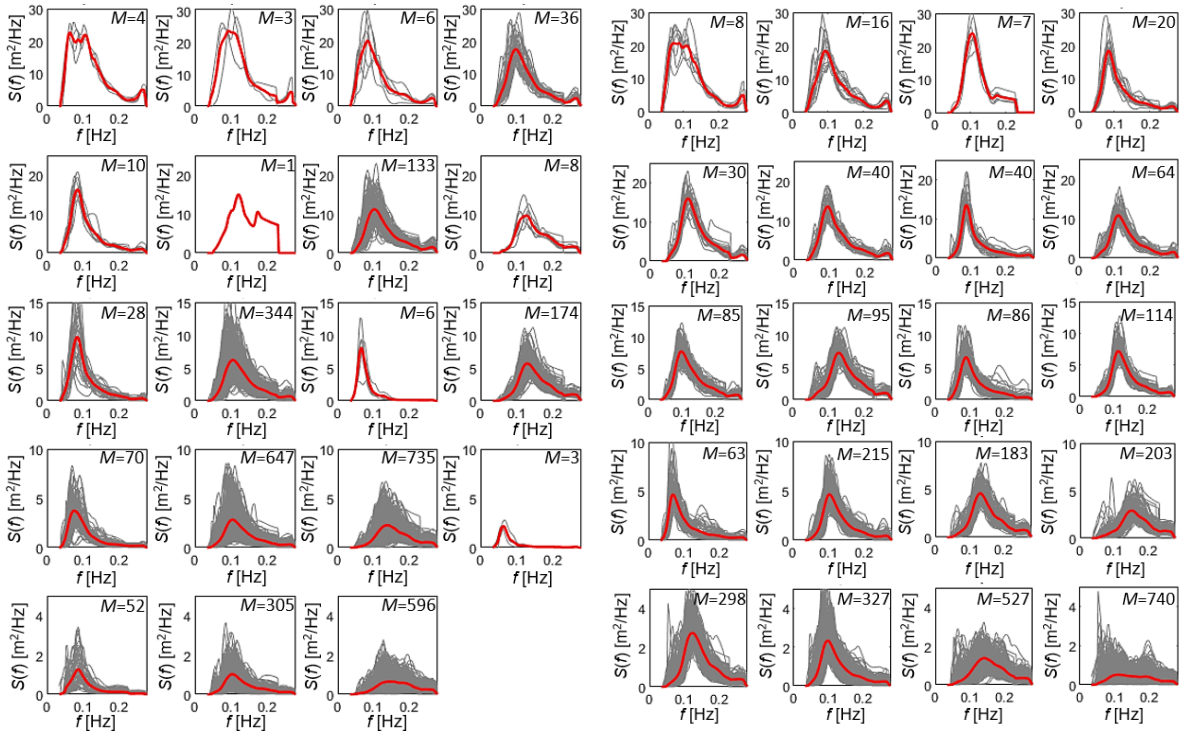

(a) (b)

Fig. 7. Comparison of method A and method C in $S(f)$ space. The members in each group are plotted with grey lines; the corresponding representative wave spectrum is marked in red and the parameter M represents the number of members in each group. (a) Method A. (b) Method C.

2.4. Representative sea states by method C for model testing

Since the regrouping method C has been selected to create representative sea states for physical model testing, it is then necessary to decide how many sea states can be tested with a limited time and resources. From previous work [16], the annual energy outputs determined using representative sea states with a small $K = 2$ and a large $K = 170$ are very close to each other (less than 1% difference), for a fully linear RM3 WEC model investigated numerically in WEC-Sim. To further understand the application of regrouping methods and suggest the appropriate selection of K, the representative sea states identified from method C with different K values were tested both experimentally and numerically with a 1:25 scale model hinged raft WEC.

The hourly HF radar measured data at full scale is converted to 12 minutes time duration wave series for the physical model tank testing, based on the Froude scaling law with a length scaling of 25. The time available for the model tests is 3 weeks, and considering the time needed for wave calibration and wave settling time between cases, only a limited number of representative sea states may be tested with different K. After consideration, the representative sea states used for model testing are $K = 1$, 5, 10, and 15. There are in total 31 wave cases. The

representative sea states with different K using regrouping method C are shown in Fig. 8 both in H_s-T_e space and $S(f)$ space. These obtained non-directional wave spectra as shown in Fig. 8(b) are scaled down based on the length scaling of 25 and then imported into the paddle system of the basin at the UoP and the WEC-Sim numerical model to produce the 12 minutes wave series for action on the hinged raft WEC.

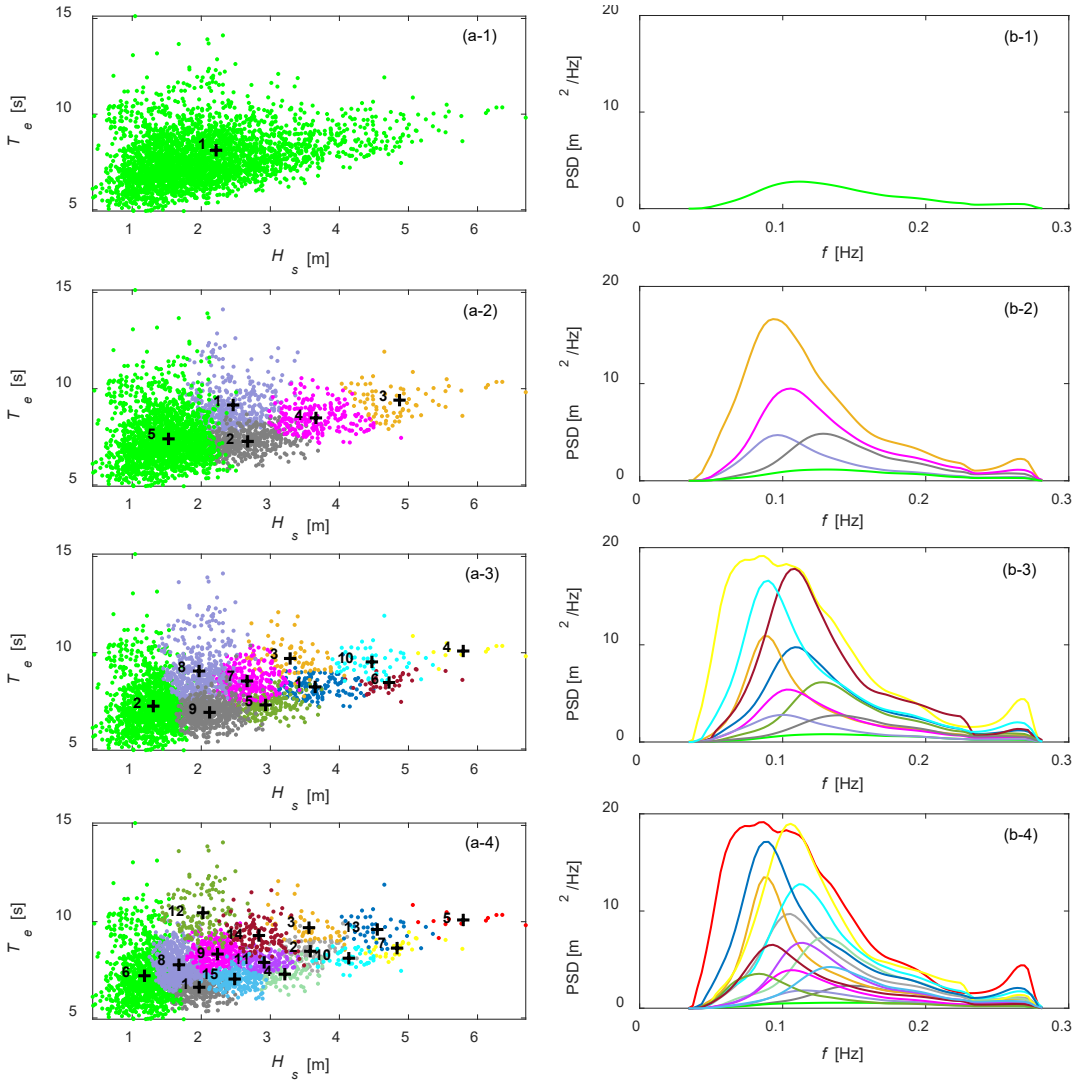

Fig.8. Full-scale representative sea states for HF radar data at Wave Hub obtained using regrouping method C. (a) H_s-T_e space. (a-1) to (a-4) represent results obtained under K = 1, 5, 10 and 15, respectively. The sea states from the same group are marked in the same color and the displayed values represent the group number k. The representative sea states are marked with black '+'. (b) $S(f)$ space. (b-1) to (b-4) represent results obtained under K = 1, 5, 10 and 15, respectively. The representative non-directional wave spectra are marked in solid lines using the same group color described in H_s-T_e space.

3. Description of the physical and numerical model testing

3.1. Physical model testing

The physical model testing took place in the ocean basin of the COAST lab at UoP. Detailed parameters of this basin can be found in [26]. The geometry of the 1:25 hinged raft WEC and the layout of the physical tank testing are described in Fig. 9. The key parameters of the WEC are shown in Table 3.

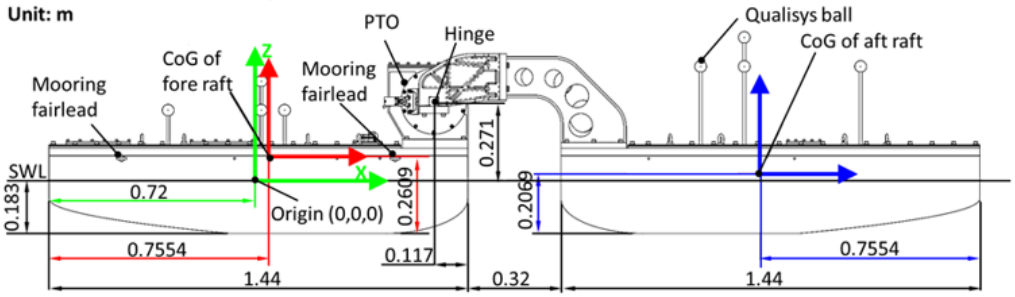

(a)

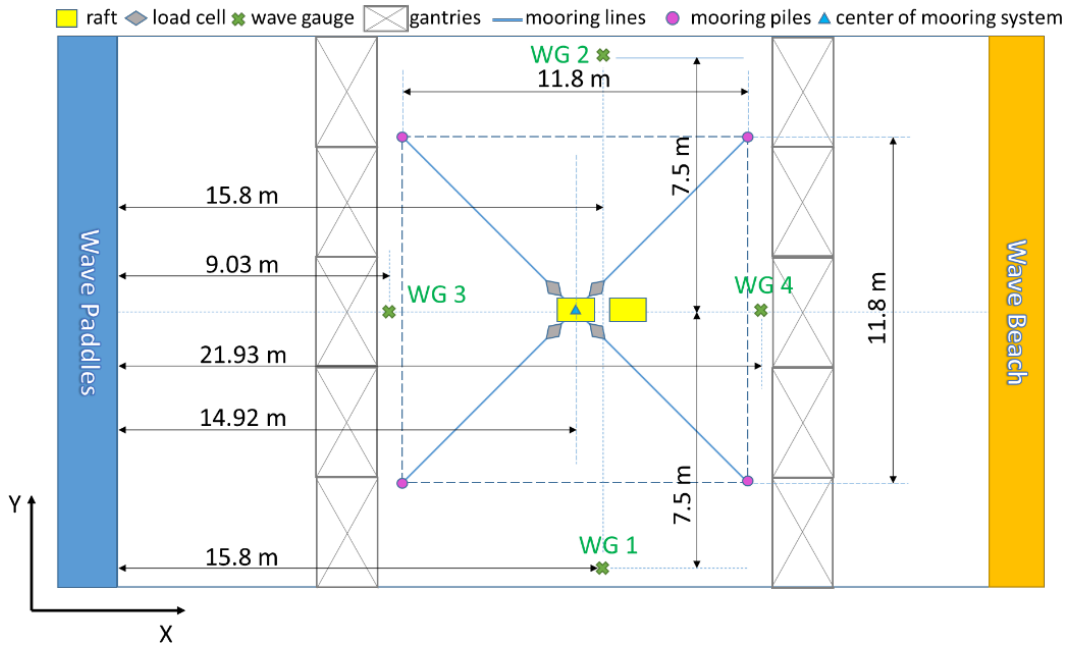

(b)

Fig. 9. (a) Schematic of the 1:25 hinged raft WEC. (b) The plan view of the physical model testing in the wave basin at the UoP. The water depth is set at 3 m.

Table 3: Main parameters for the 1:25 hinged raft WEC. The order of the inertias is I_{XX}, I_{YY}, I_{ZZ}.

Measure	Unit	Value
Length overall	m	3.2
Length fore raft	m	1.44
Length aft raft	m	1.44
Draft	m	0.183
Width	m	0.87
Mass overall	kg	399.5
Mass front raft	Kg	199.8
Mass back raft	Kg	199.7
Inertias of fore raft	kgm^2	15.75, 66, 71.5
Inertias of aft raft	kgm^2	15.75, 66, 71.5
PTO rotational damping	Nms/rad	20
Spring stiffness	N/s	28

As shown in Fig. 9, this WEC model has two rafts connected by a hinge. There is a motor in the hinge that controls the rotational damping parameter. It provides a linear PTO with a rotational damping parameter of 20 Nms/rad. There are four aerial mooring lines (parallel to the water surface without touching) with a 90° interval to hold the position of the device during tank testing which make this hinged raft WEC always face the direction of the incident wave and thus it is not sensitive to the wave direction. Each of the mooring lines consists of a rope and a tension spring with a linear stiffness of 28 N/m. Two recording systems were installed on the device, which is the Qualisys motion capture system and the in-built recording system. The Qualisys system records the motions of the rafts by the markers (i.e., the Qualisys balls shown in Fig. 8(a)) mounted on the rafts. The in-built recording system consists of a series of sensors inside the rafts to measure the inner temperature, the relative hinge angle between the rafts, the rotational angular velocity of the hinge, the torque generated from the PTO, and the tension forces on the 4 mooring lines. Under the excitation of the incident wave, the fore raft and aft raft generate instantaneous relative hinge angle to drive the PTO to produce torque, which is used to simulate the generator.

Four wave gauges around the WEC were installed to measure the wave elevations. The 31 representative wave spectra obtained by regrouping method C shown in Fig. 8(b) were calibrated in the ocean basin before running

the physical model tests with the WEC. Each of the waves was measured before the model installation at the position of the hinge with a wave gauge. The measured waves were transferred into the wave spectrum using Direct Fourier Transformation (DFT) and compared with the target wave spectrum. The difference between the target and the measurement was used to calibrate the input wave signal. After calibration, all of the 31 wave cases are within 5% relative error of the target wave spectra. Fig. 10 shows one representation of the wave calibration.

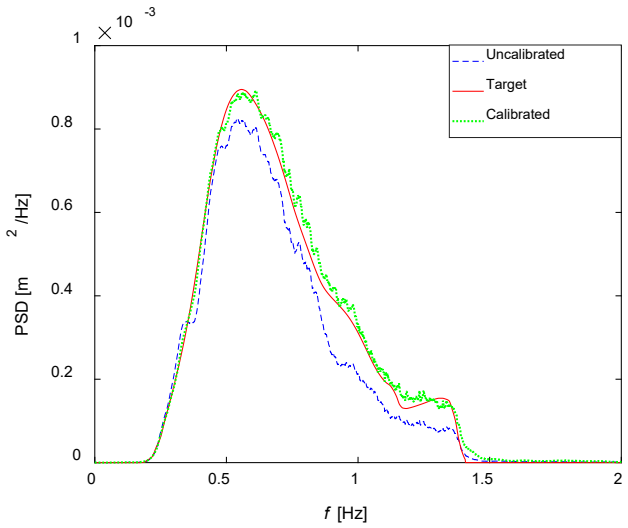

Fig. 10. The calibration result of one wave spectrum from the 31 representative waves (see Fig. 8(b)) tested in the ocean basin at the UoP.

3.2. Numerical model testing in WEC-Sim

In order to compensate for the time limit of the physical model testing in which only method C was evaluated, numerical testing is also conducted in this work to provide more insight on comparing different regrouping methods A to J for WEC model testing. Here, WEC-Sim is used to conduct the numerical testing, as shown in Fig. 1(b). WEC-Sim, an open-source tool developed and released by the National Renewable Energy Laboratory (NREL) and Sandia National Laboratory (SNL) in 2014, has been widely used to model different types of WEC, such as the PA, Oscillating Water Column (OWC) and oscillating wave surge converter [27]. However, there exist few studies of modelling a hinged raft WEC in WEC-Sim. Therefore, one target of the Supergen ORE Hub project is to develop and validate nonlinear WEC-Sim model for the hinged raft type WEC with physically observed nonlinearities considered. Based on this 1:25 hinged raft WEC tested in the physical tank, a nonlinear WEC-Sim model has been developed and validated. The corresponding work has been submitted and is under revision based on the reviewers' comments. In this work, the developed and validated nonlinear WEC-Sim numerical model of

this 1:25 hinged raft is used to conduct the study of comparing different regrouping method. A quadratic viscous term in Morison equation is validated by the physical tank testing data and built into the WEC-Sim numerical model, in order to represent the nonlinear fluid viscous effect observed from the physical tank testing. Details of developing nonlinear WEC numerical model induced by fluid viscous effect can be found in [28]. It should be noted that different from using a linear numerical RM3 WEC-Sim model to assess the performance of the regrouping method [16], the hinged raft WEC-Sim model used in this work shows clear non-linearity, which will be discussed in the latter part of this section.

Taking method C with $K = 15$ as an example, Fig. 11 clearly describes the representative waves input into WEC-Sim for numerical model testing at a 1:25 model scale and the waves are obtained by scaling down the data shown in Fig. 8, using the length scaling factor of 25. As can be seen, the K-means clustering method results in similar sea states in the same groups. Additionally, the group created with $k = 6$ has the largest number of members inside with $M = 928$, taking up to 29.4% of the total 3161 sea states, while it also represents one of the most modest sea states. Conversely, group $k = 5$ has the smallest number of members inside with $M = 13$, but represents one of the most severe wave conditions. Fig. 12 plots the obtained physical and numerical response amplitude operators (RAOs) in relative hinge angle under the representative wave conditions for $k = 5$ and 6, as well as $k = 9$ and 13.

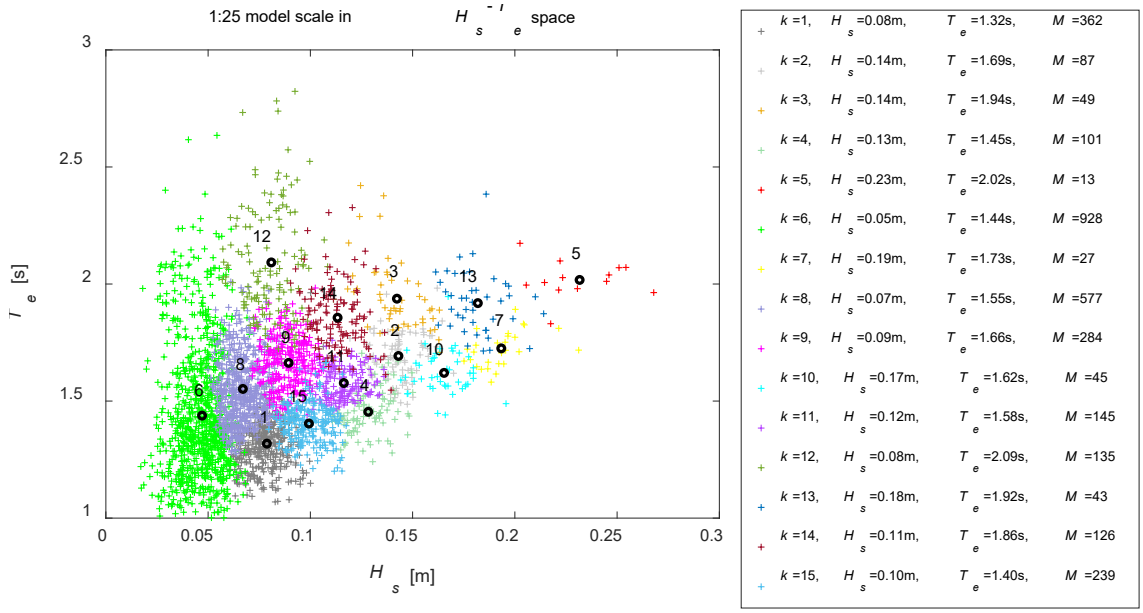

(a)

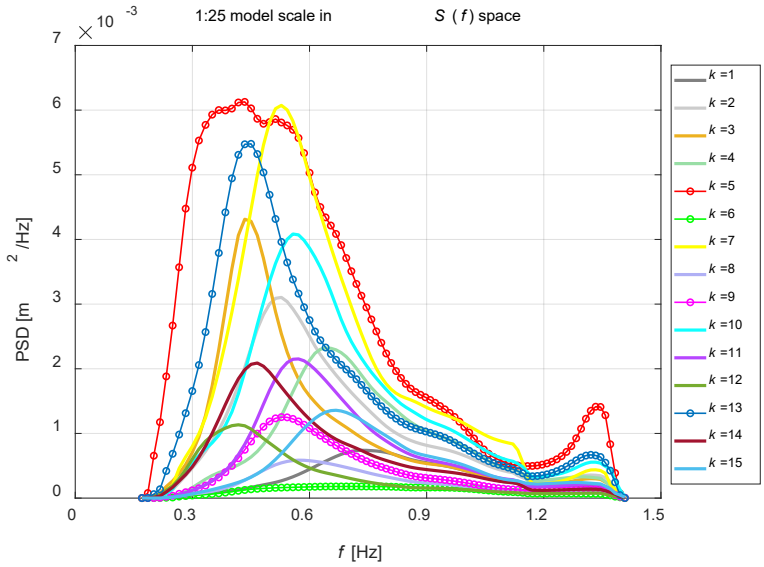

(b)

343 Fig.11. Representative waves imported into the 1:25 scale WEC-Sim model under method C with $K = 15$. (a) H_s-
344 T_e space. The sea states from the same group are marked in the same colour and the black circles are the 15
345 representative waves. The black numbers represent the group number k. Parameter M represents the number of
346 members in group k. (b) $S(f)$ space.

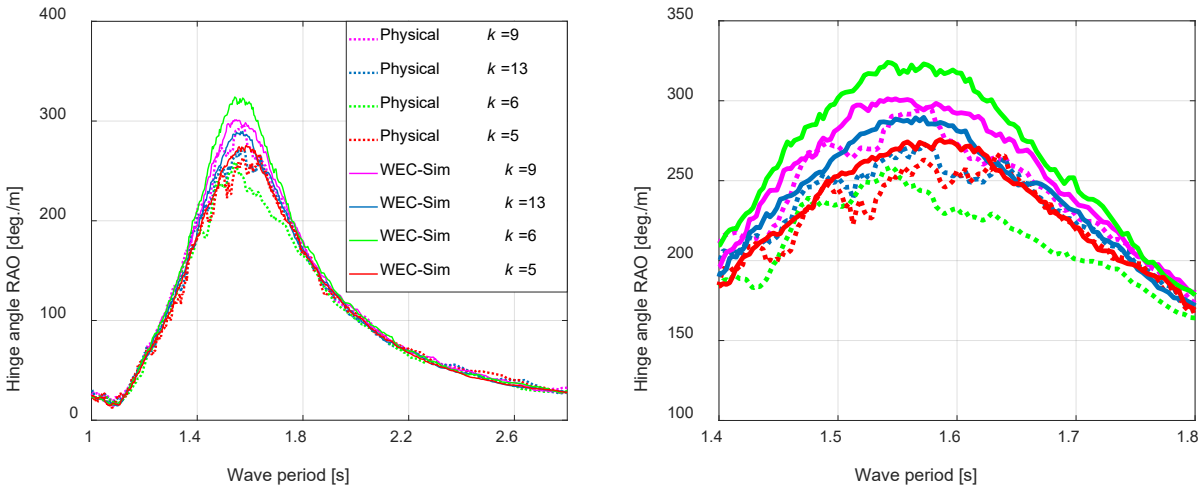

347 Fig.12. Physical and numerical RAOs in relative hinge angle for the smallest and largest number of representative
348 sea states under $k = 5$ ($H_s = 0.23$ m and $T_e = 2.02$ s) and $k = 6$ ($H_s = 0.05$ m and $T_e = 1.44$ s), as well as $k = 9$ (H_s
349 $= 0.09$ m and $T_e = 1.66$ s) and $k = 13$ ($H_s = 0.18$ m and $T_e = 1.92$ s). The left figure shows the results in full range
350 and the right shows the close-up.

351 As can be seen from Fig. 12, the physically and numerically observed resonance in relative hinge angle happens
352 at wave period of 1.54 s to 1.60 s. Additionally, the numerical/physical RAO lines vary with different wave periods,

which confirms that the device performs nonlinearly. For numerical WEC-Sim results (solid lines), it can be seen clearly that the RAO peak decreases with increasing H_s. A similar trend is observed physically, under k = 5, 9, and 13. The exception is for k = 6 (green dotted line) for which the smallest H_s of 0.05 m does not generate the highest RAO peak as that obtained numerically. The reason may be that it is relatively hard to calibrate the wave accurately when H_s is quite small in the physical basin. In addition, as described in Table 3, the mass and size of this hinged raft WEC are significant compared to the small H_s of 0.05 m. Therefore, the physical response may be contaminated by uncertainties such as the free surface not fully settling between wave cases and the reflection in the physical basin, especially under small waves, which are, however, absent in the numerical WEC-Sim model. As observed, under k = 5, 9, and 13 with larger H_s, the numerical results (red, pink, and blue solid lines) match those from physical tests (red, pink, and blue dotted lines) well, with just slight over predictions.

For the total 31 representative wave cases under K = 1, 5, 10, and 15 generated by method C, the numerically and physically obtained power outputs are summarised in Table 4. Detailed formulae for evaluating the power output are expressed below:

$$M_{PTO}(t) = -B_{PTO}\dot{\theta}(t), \tag{7}$$

$$P_{PTO}(t) = M_{PTO}(t)\dot{\theta}(t), \tag{8}$$

$$\bar{P} = \frac{1}{T_2 - T_1}\int_{T_1}^{T_2} P_{PTO}(t)dt, \tag{9}$$

$$e = \frac{\bar{P}_{num} - \bar{P}_{phy}}{\bar{P}_{phy}} \times 100\%, \tag{10}$$

where M_{PTO} is the instantaneous torque generated at the hinge. For physical model testing, M_{PTO} was directly measured by the in-built torque metre. For the WEC-Sim numerical model, it was calculated by Eq. (7). B_{PTO} is the rotational damping parameter; $\dot{\theta}(t)$ is the angular velocity of the relative pitch angle; P_{PTO} is the instantaneous power; $\bar{P}$ is the average power where T_1 and T_2 are the start and end time for the analysis of a test case; e is the relative error between the physical and numerical results.

As can be seen from Table 4, the numerical and physical results agree with each other well. Using ±15% relative error limit as the boundary, for K = 1, the error for the only representative sea state is only 7.076%, within the boundary; 1 out of 5 cases for K = 5, 2 out of 10 cases for K = 10, and 3 out of 15 cases for K = 15 exceed the boundary with the highest error of 32.175%. As observed, these 6 sea states with errors out of the boundary are from the largest groups for a certain K value. For K = 5, it is the group k = 5 with 1939 members (61.3%) out of 3161. For K = 10, they are the group k = 2 with 1310 (41.4%) and group k = 8 with 468 (14.8%) members

respectively. For K = 15, they are group k = 1 with 362 (11.5%), group k = 6 with 928 (29.4%) and group k = 8 with 577 (18.3%) members. From Fig. 8, it can be seen clearly that all of these large groups are with small representative waves of H_s < 0.08 m under the model scale. As discussed before, the physical response can be highly affected by the water surface not being fully calm between wave cases and the reflection under small wave conditions. This explains why the representative sea state tested physically with a small target H_s has a large relative error with the numerical result of the average power output compared with large waves.

Overall, the validated non-linear WEC-Sim model can represent the physically observed performance of this device well and is used in this work.

Table 4: The obtained physical and numerical average power outputs for method C with K = 1, 5 10, and 15.

K	k	M	$\bar{P}_{phy}$ [W]	$\bar{P}_{num}$ [W]	e [%]	k	M	$\bar{P}_{phy}$ [W]	$\bar{P}_{num}$ [W]	e [%]
1	1	3161	1.32	1.41	7.08					
5	1	424	1.36	1.51	11.59	4	221	3.25	3.53	8.77
	2	496	2.26	2.37	4.98	5	1939	0.58	0.67	15.04
	3	81	4.63	5.05	8.99					
10	1	143	3.47	3.81	10.05	6	36	5.55	5.88	6.04
	2	1310	0.36	0.48	32.18	7	262	1.96	2.02	3.23
	3	78	1.92	2.04	6.21	8	468	0.86	1.01	17.25
	4	13	6.00	6.45	7.48	9	565	1.26	1.40	11.67
	5	232	2.74	2.95	7.55	10	54	3.69	3.81	3.11
15	1	362	0.92	1.09	18.12	9	284	1.61	1.57	-2.16
	2	87	3.19	3.36	5.46	10	45	4.57	4.82	5.50
	3	49	2.31	2.39	3.38	11	145	2.70	2.83	4.91
	4	101	3.23	3.45	6.63	12	135	0.65	0.74	14.46
	5	13	6.03	6.42	6.45	13	43	3.76	3.91	4.00
	6	928	0.26	0.35	31.44	14	126	1.69	1.83	8.00
	7	27	5.61	5.84	3.99	15	239	1.98	2.11	6.50
	8	577	0.82	0.94	15.70					

4. Results and discussion of WEC performance estimation using different regrouping methods

The effect of different regrouping methods on WEC performance estimation is evaluated. Only two parameters are used to discuss the WEC performance, including total energy output and average power output in this work.

4.1. Impact of *K*

As suggested in [15], increasing *K* (number of groups) can improve the wave regrouping quality and convergence can be reached at *K* = 20. This highlights that 20 selected representative waves can be used to efficiently represent a large wave dataset. It is well known that the WEC performance is the interaction between the wave and the device. Therefore, it would be questionable whether the 20 representative waves (as given in Fig. 5) can give high representativeness in estimating WEC performance.

Here, the impact of *K* on the WEC performance estimation is evaluated by the total energy generated for this hinged raft WEC. The total energy generation is expressed as:

$$E_k = \bar{P}_k \times M(k) \times 720, \tag{11}$$

$$E_{total} = \sum_{k=1}^{K} E_k, \tag{12}$$

where $\bar{P}_k$ (Eqs. (7) to (9)) is the average power output from the representative sea states of group *k* under the 1:25 scale. *M*(*k*) is the number of members inside group *k*. The time used to calculate energy output is 720 s related to the one-hour duration in full scale. E_{total} is the total energy output estimated under the 1:25 scale for a defined *K*.

In addition, the accurate total energy $E_{accurate}$ using the total 3161 hourly HF radar dataset without using any regrouping methods is calculated as the baseline counterpart. It is impractical to run 3161 cases in a physical ocean basin to obtain $E_{accurate}$, while it is available to run the validated WEC-Sim numerical model. Then, $E_{accurate}$ can be obtained from:

$$E_{accurate} = \sum_{i=1}^{3161} \bar{P}_i * 720, \tag{13}$$

in which $\bar{P}_i$ is the average power output of each of the 3161 sea states under the 1:25 model scale.

Table 5: The physical and numerical total energy output for method C with different K in full scale.

K	Physical E_{total} [kW·h]	Numerical E_{total} [kW·h]	e [%]
1	325962.8	349028.8	7.08
5	306085.9	336495.7	9.94
10	301319.3	336701.3	11.74
15	311106.4	338461.6	8.79

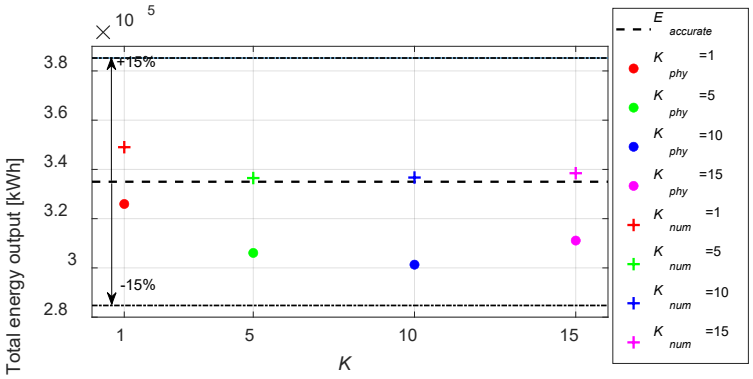

Fig. 13. Impact of different K on predicting the performance of the hinged raft WEC prototype according to total energy output under regrouping method C, investigated physically and numerically. $E_{accurate}$ = 334997.9 kW·h. The two black dash-dotted lines are the ±15% relative error limits with reference to $E_{accurate}$.

Table 5 and Fig. 13 summarise the predicted total energy outputs generated by using regrouping method C with K = 1, 5, 10, and 15, as well as the accurate total energy. It should be noted that the energy outputs presented are converted into full scale by scaling factor 25^4.

As shown in Table 5, the numerical total energy outputs predicted using the WEC-Sim model are quite close to those obtained from physical model testing under K = 1, 5, 10, and 15 with the relative errors limited by 11.742%. As seen from Fig. 13, the deviations of numerical/accurate and physical/accurate are small within 15% for K = 1, 5, 10, and 15. Furthermore, there exists no significant trend showing that increasing K can reduce the deviation between the total energy estimation and the accurate energy. To quantify this, for the total energy output from physical model testing, the average value with K = 1, 5, 10, and 15 is 3.11×10^5 kW·h with a standard deviation (STD) of 1.07×10^4 kW·h. The coefficient of variation (STD/mean) is 3.4%, which means the variation of the annual energy output estimation from different K values is small. For the total energy output from numerical model testing, the average value with K = 1, 5, 10, and 15 is 3.40×10^5 kW·h; the STD is 5.97×10^3 kW·h and the

coefficient of variation is only 1.76%. Therefore, it can be suggested that the influence of K value on the total energy output prediction is not significant, according to the hinged raft WEC studied in this work. In other words, the annual energy output can be accurately predicted by using just a few representative sea states with $K \leqslant 15$, although the 1:25 hinged-raft numerical model is non-linear.

This is partially due to the fact presented in Fig. 14 together with the results presented in Table 4. The hinged raft WEC studied in this work is not optimally designed for the Wave Hub site. The device performs as a 'wave rider' with low power outputs for most waves, with a quite narrow resonance range (period of 1.54 s to 1.60 s) in which only 254 out of 3161 waves exist. Therefore, the calculation of total energy output for this device is highly dependent on the waves with a large number of occurrences but low power outputs, but not the waves for high power outputs and considerably low occurrences. From Fig. 14, it can be expected that even if a WEC model with much larger nonlinearity is used, the influence of the nonlinearity on the annual energy output is limited. It is because compared to the total number of annual hourly sea states, the number of sea states that can cause the resonance of the WEC is very small. It is necessary for the WEC to be resonated in a much wider range of T_e in order for the nonlinearity to have a large effect on the annual energy output prediction. However, this hinged-raft model only resonates in a very narrow range of T_e. As a result, the total energy output prediction is not sensitive to K. It means that regardless of the linearity of the WEC model, by using the K-means clustering method with a small number of K, the total energy output can be accurately predicted. This finding is similar to that based on the fully linear RM3 WEC-Sim model for the Wave Hub site [16]. In future work, it is necessary to test the impact of K according to a well-designed WEC for a considered ocean field with a broader resonance range achieved (e.g. WECs with adjustable resonance range or dual-resonance WECs [29]).

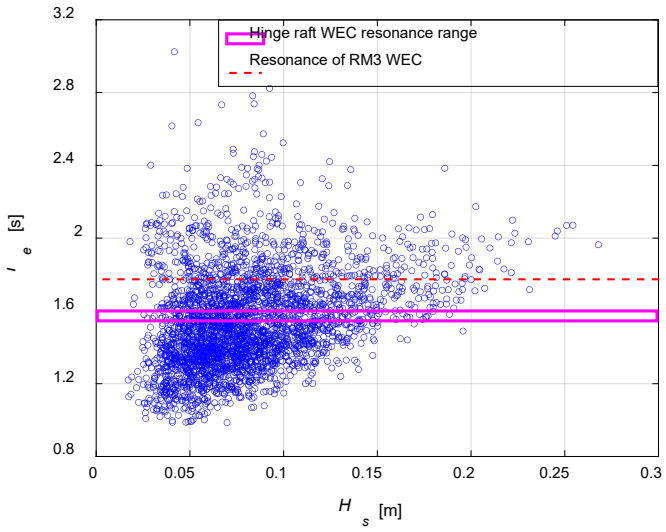

Fig. 14: Resonance range of the hinged raft WEC and the RM3 WEC for the Wave Hub site.

4.2. Total energy output representativeness using different regrouping methods.

Next is to compare the total energy prediction using different regrouping methods A to J. The study is conducted through the validated WEC-Sim model of the 1:25 hinged-raft. For each regrouping method, K = 20 is used, i.e., the 20 representative sea states given in Fig. 5 are imported into the numerical model to obtain the corresponding total energy output (via Eqs. (7) to (12)). The obtained results are summarised in Table 6.

From the results, it can be noticed that the methods using K-means clustering (C to I) show a clear improvement of representativeness in predicting total energy output compared to the binning methods (A and B), by reducing the relative errors.

Table 6: Total energy prediction from different regrouping methods for the hinged raft WEC in full scale and the errors relative to the accurate total energy generation.

Method	E_{total} [kW·h]	$E_{accurate}$ [kW·h]	Relative error [%]
A	338978.7	334997.9	1.19
B	338569.4	334997.9	1.07
C	336297.7	334997.9	0.39
D	335957.5	334997.9	0.29
E	335336.3	334997.9	0.10
F	337069.9	334997.9	0.62
G	334755.2	334997.9	0.07
H	337094.5	334997.9	0.63
I	335090.1	334997.9	0.03
J	338846.5	334997.9	1.15

4.3. Power output representativeness analysis with different regrouping methods.

In addition to the total energy output, the average power representativeness of the device is evaluated for different regrouping methods with K = 20. The obtained representative sea states from each regrouping method (as shown

in Fig. 5) are imported into the validated WEC-Sim model to obtain the corresponding average power outputs under k = 1, 2, 3 … 20.

The WEC's average power outputs of the total 3161 hourly sea states can be calculated using the WEC-Sim model. Then, the metric values for the device's power output representativeness regarding methods A to J can be carried out (using Eq. (6)), as summarised in Fig. 15. For comparison, the metric values of wave power P_w for the HF radar dataset (as given in Fig. 6) and the device power output metric values from the fully linear RM3 WEC [16] are also plotted.

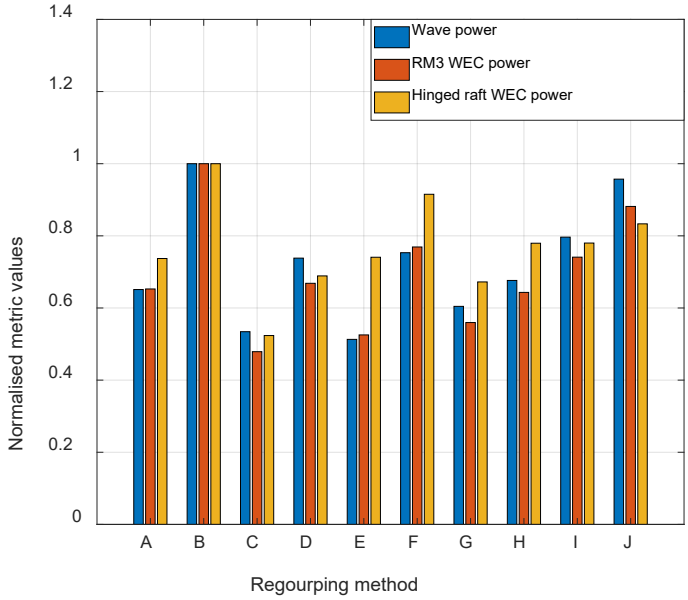

Fig. 15: Comparison of the normalised metric values (normalised by the highest values) from wave power of the HF radar dataset, the RM3 WEC power output, and the power output of the hinged raft WEC studied in this work. The used representative sea states are shown in Fig. 5.

Overall, it can be found that method C performs the best, giving relatively low metric values not only for the wave power of Wave Hub but also for the power output predictions of the two WEC devices. This highlights that the representative sea states from method C (as shown in Fig. 5) provide the wave power of Wave Hub and also the average power output estimations for the two WEC devices with the highest representativeness. Therefore, method C using *K*-means clustering is more recommended for conducting model testing to predict power outputs of the two WEC devices for the Wave Hub site, instead of the widely used binning method (A/B).

Additionally, it can be noticed that the metric values for the wave power and the power prediction of the RM3 WEC from different grouping methods are similar, showing the same descending order of B > J > I/F > D > A/H >

G > E/C. By contrast, the metric values of different regrouping methods for the hinged raft show significant difference with descending order of B > F > J > I > H > E > A > D > G > C. This is because the two WEC devices are completely different and the fully linear RM3 WEC performs more like a 'wave rider' compared to the hinged raft WEC for the most common conditions at Wave Hub (see Fig. 14). Therefore, the representative wave power from different regrouping methods can be directly reflected on the average power output prediction of the fully linear RM3 WEC, but not the hinged raft WEC which has relatively stronger wave-device interaction and nonlinear performance, as clarified in Figs. 12 and 14.

This in turn emphasizes that if a studied WEC performs not as a 'wave rider' and could achieve resonance frequently with a broader resonance range for a specific ocean area (e.g. WECs with adjustable resonance range or dual-resonance WECs [29]), the representative waves obtained to highly represent the characteristics of waves for the site could be different from the most representative waves used to predict the WEC performance. Overall, it is suggested to conduct the analysis considering the specific WEC performance (such as power output, energy generation, fatigue, etc.) to obtain the most representative sea states for the model testing of a WEC device.

5. Conclusion

First, obtaining a small number of sea states but with high representativeness is considered important for conducting model testing of a WEC at the design stage efficiently. The *K*-means clustering method is investigated and compared to the widely used binning method in this work. The 3161 HF radar measured wave data for the Wave Hub, the UK in 2012 is used as the wave dataset. 10 regrouping methods A-J are developed to achieve representative sea states for the Wave Hub Site. It is found that method C using the *K*-means clustering technique can generate the representative sea states, highly preserving the real wave characteristics. T It should be noted that this finding is irrelevant to WECs. To further show the benefit of K-means clustering method in WEC model testing, the obtained representative sea states were then tested on a WEC.

A 1:25 designed hinged raft WEC model was tested experimentally and numerically. The numerical model is developed in the open-source tool WEC-Sim with validation by experimental data. To the best knowledge of the authors, this is the first time that regrouping methods from both *K*-means clustering and the binning method are thoroughly compared on a WEC with the use of the HF radar measured physical data.

Both the physical and the validated WEC-Sim numerical results show that the 1:25 hinged-raft model is non-linear. However, the influence from non-linearity is limited for the Wave Hub site due to the fact that most of the sea states are with T_e outside of the resonance range of the model. As a result, it was found that the total energy

output can be accurately predicted using a small number of representative sea states from method C with $K \leqslant 15$. In addition, it was found that using the *K*-means clustering method not only improves the sea states with higher representativeness but also improves the device power output and total energy generation with higher representativeness, compared to the traditional binning method.

Method C, using *K*-means clustering with non-directional wave spectrum, is preferred to obtain the representative sea states for the average power output estimation of the WECs with little influence from wave direction such as the hinged raft studied here and the RM3 point absorber WEC in [16]. Overall, the methodology developed and validated in this work provides more insight into the use of the *K*-means clustering method for the design of model tests. In the future, WECs which are sensitive to incoming wave directions need to be analysed. WECs with a broader resonance range or dual resonance peaks need to be analysed as well to see the influence of group number *K* on the annual energy prediction of the device. Additionally, the representative sea states obtained are for operational wave conditions. It is expected to use the *K*-means technique in the future to obtain extreme wave conditions.

CRediT authorship contribution statement

Daming Wang: Conceptualization, Methodology, Investigation, Writing - original draft. **Siya Jin**: Conceptualization, Methodology, Software, Investigation, Validation, Writing - original draft. **Martyn Hann:** Conceptualization, Investigation, Supervision, Writing - review & editing. **Keri Collins:** Supervision, Writing - review & editing**. Daniel Conley:** Supervision, Writing - review & editing. **Deborah Greaves:** Conceptualization, Supervision, Funding acquisition, Writing - review & editing.

Acknowledgements

This research is conducted as part of the EU funded MaRINET 2 project (grant agreement ID: 731084) and the EPSRC funded Supergen ORE Hub (EP/S000747/1). The authors would also like to thank the ECN for designing and manufacturing the model and the technicians in UoP for the support during the tank testing.

Reference

1. Mørk, G., et al. *Assessing the Global Wave Energy Potential*. in *29th OMAE*. 2010. https://10.1115/omae2010-20473. Accessded on 01/12/2021.
2. Statista. *Electricity generation worldwide from 1990 to 2021*. Available from: https://www.statista.com/statistics/270281/electricity-generation-worldwide/.
3. Falcao, F.d.O., Antonio, *Wave energy utilization: A review of the technologies.* Renew Sustain Energy Rev, 2010. **14(3)**: p. 899-918. https://doi.org/10.1016/j.rser.2009.11.003.

4. Henderson, R., *Design, simulation, and testing of a novel hydraulic power take-off system for the Pelamis wave energy converter.* Renew Energy, 2006. **31**(2): p. 271-283. https://doi.org/10.1016/j.renene.2005.08.021.
5. Santo, H., P.H. Taylor, and P.K. Stansby, *The performance of the three-float M4 wave energy converter off Albany, on the south coast of western Australia, compared to Orkney (EMEC) in the U.K.* Renew Energy, 2020. **146**: p. 444-459. https://doi.org/10.1016/j.renene.2019.06.146.
6. Draycott, S., et al., *Re-creation of site-specific multi-directional waves with non-collinear current.* Ocean Engineering, 2017.
7. *Mocean Energy. https://www.mocean.energy/wave-energy-converter. Accessed on 18/12/2021.*
8. Héder, M., *From NASA to EU: the evolution of the TRL scale in Public Sector Innovation.* The Innovation Journal, 2017. **22**(2): p. 1-23. https://www.researchgate.net/publication/350942366_From_NASA_to_EU_the_evolution_of_the_TRL_scale_in_Public_Sector_Innovation. Accessed on 11/12/2021.
9. Hodges, J., et al., *An international evaluation and guidance framework for ocean energy technology.* IEA-OES: Lisbon, Portugal, 2021.
10. Ingram, D.M., et al., *Protocols for the Equitable Assessment of Marine Energy Converters.* 2011. https://www.researchgate.net/publication/257409230_Protocols_for_the_Equitable_Assessment_of_Marine_Energy_Converters. Accessed on 12/12/2021.
11. Hasselmann, K., *Measurements of wind-wave growth and swell decay during the Joint North Sea Wave Project (JONSWAP).* Dtsch.Hydrogr.Z, 1973. **8**.
12. Carballo, R. and G. Iglesias, *A methodology to determine the power performance of wave energy converters at a particular coastal location.* Energy Convers Manage, 2012. **61**: p. 8-18. https://doi.org/10.1016/j.enconman.2012.03.008.
13. Hamilton, L., *Characterising spectral sea wave conditions with statistical clustering of actual spectra.* Appl Ocean Res, 2010. **32**(3): p. 332-342. https://doi.10.1016/j.apor.2009.12.003.
14. Draycott, S.T., *On the re-creation of site-specific directional wave conditions*. 2017.
15. Wang, D., et al., *Use of HF radar for replciating wave-current combined wave conditions for testing of wave energy converters*, in *13th EWTEC*. 2019. https://pearl.plymouth.ac.uk/bitstream/handle/10026.1/16004/WANG--Use%20of%20HF%20radar%20for%20replicating%20wave-current%20combined%20wave%20conditions%20for%20testing%20of%20wave%20energy%20converters%20--EWTEC2019.pdf?isAllowed=y&sequence=1. Accessed on 24/12/2021.
16. Wang, D., et al., *Power output estimation of WEC with HF radar measured complex representative sea states*, in *14th EWTEC*. 2021. https://www.researchgate.net/publication/357270518_Wang--EWTEC2021_dmg_-_revised. Accessed on 24/12/2021.
17. Draycott, S., et al., *Applying site specific resource assessment: Methodologies for replicating real seas in the FLOWAVE facility*, in *International Conference on Ocean Energy (ICOE)*. 2014.
18. Davey, T., et al., *Round Robin Testing: Exploring Experimental Uncertainties through a Multifacility Comparison of a Hinged Raft Wave Energy Converter.* J Mar Sci Eng, 2021. **9**(9): p. 946. https://doi.org/10.3390/jmse9090946.
19. Lopez, G., D.C. Conley, and D. Greaves, *Calibration, Validation, and Analysis of an Empirical Algorithm for the Retrieval of Wave Spectra from HF Radar Sea Echo.* Journal of Atmospheric and Oceanic Technology, 2015. **33**(2): p. 245-261.
20. Han, J., M. Kamber, and J. Pei, *Data mining: Concepts and techniques*. 2006, Morgan Kaufmann.
21. Arthur, D. and S. Vassilvitskii, *k-means++: The advantages of careful seeding*. 2006, Stanford.
22. Spath, H., *The cluster dissection and analysis theory fortran programs examples*. 1985: Prentice-Hall, Inc.
23. Fränti, P. and S. Sieranoja, *How much can k-means be improved by using better initialization and repeats?* Pattern Recognition, 2019. **93**: p. 95-112.
24. Draycott, S., et al. *Applying site specific resource assessment: methodologies for replicating real seas in the FloWave facility*. 2014. ICOE.

25. Draycott, S., et al., *Applying Site-Specific Resource Assessment: Emulation of Representative EMEC seas in the FloWave Facility*. International Society of Offshore and Polar Engineers.
26. Rodriguez, M., J. Spinneken, and C. Swan, *Nonlinear loading of a two-dimensional heaving box.* Journal of Fluids and Structures, 2016. **60**: p. 80-96.
27. Yu, Y.-H., et al., *Review of WEC-Sim Development and Applications*. 2020, Sandia National Lab.(SNL-NM), Albuquerque, NM (United States).
28. Jin, S., R.J. Patton, and B. Guo, *Viscosity effect on a point absorber wave energy converter hydrodynamics validated by simulation and experiment.* Renewable energy, 2018. **129**: p. 500-512.
29. Chen, Z., et al., *Experimental and numerical study on a novel dual-resonance wave energy converter with a built-in power take-off system.* Energy, 2018. **165**: p. 1008-1020.